IEEE Open Journal of Signal Processing

Received 19 March 2023; accepted 10 May 2023. Date of publication 22 May 2023;
date of current version 14 June 2023. The review of this article was arranged by Associate Editor Danilo Orlando.

Digital Object Identifier 10.1109/OJSP.2023.3278593

Sparse Billboard and T-Shaped Arrays for Two-Dimensional Direction of Arrival Estimation

SALEH A. ALAWSH [1] (Member, IEEE), MOHAMED H. MOHAMED [2], IBRAHIM ABOUMAHMOUD [2], MOHAMMAD ALHASSOUN [3] (Member, IEEE), AND ALI H. MUQAIBEL [3] (Senior Member, IEEE)

[1]Center for Communication Systems and Sensing, King Fahd University of Petroleum and Minerals, Dhahran 31261, Saudi Arabia
[2]Electrical Engineering Department, King Fahd University of Petroleum and Minerals, Dhahran 31261, Saudi Arabia
[3]Electrical Engineering Department and Center for Communication Systems and Sensing, King Fahd University of Petroleum and Minerals, Dhahran 31261, Saudi Arabia

CORRESPONDING AUTHOR: SALEH A. ALAWSH (e-mail: salawsh@kfupm.edu.sa).

This work was supported by the Deanship of Research Oversight and Coordination at King Fahd University of Petroleum & Minerals through the Interdisciplinary Research Center for Communication Systems and Sensing.
This article has supplementary downloadable material available at https://doi.org/10.1109/OJSP.2023.3278593, provided by the authors.

ABSTRACT In two-dimensional direction of arrival (2D-DOA) estimation, planar arrays can estimate the elevation and azimuth angles simultaneously. However, many planar array topologies such as billboard, L-shaped, T-shaped, and 2D nested arrays suffer from mutual coupling that results from the small separation between the physical sensors (antennas), which limits the estimation capability of the sensor array. In an attempt to reduce mutual coupling between sensors, this article proposes sparse billboard and T-shaped arrays in which the number of closely separated sensors is significantly reduced. In addition to extending the CRB for fourth order coarray, this article also derives closed-form expressions for the sensor locations and the number of consecutive lags or the uniform degrees of freedom (uDOF), in the fourth-order difference coarray (FODC). Simulation results demonstrate the robustness of the proposed sparse arrays against mutual coupling.

INDEX TERMS 2D-DOA estimation, billboard arrays, fourth-order difference coarray, mutual coupling, second-order difference coarray, sparse arrays, T-shaped arrays, uniform degrees of freedom.

I. INTRODUCTION

Direction of arrival (DOA) estimation has many applications in array processing and communication systems. A key aspect of a DOA system is the antenna array topology that fits the required specifications. Antenna arrays can be classified into one-dimensional (1D), two-dimensional (2D), or three-dimensional (3D) arrays, and each type can be further classified into sparse or uniform. Uniform 2D arrays include the uniform rectangular array (URA) [1], uniform circular array (UCA) [1], cross-shaped array [2], [3], [4], and the L-shaped array [5], [6], [7], [8]. The L-shaped array is widely investigated in the literature and some authors proposed to replace the two uniform linear subarrays (legs) with sparse arrays [6], [7], [8], [9], [10], [11].

There are several metrics to compare 2D sparse arrays, including but not limited to: number of virtual lag locations, required aperture size, resolution, and mutual coupling. Researchers focused on proposing configurations that have closed-form expressions for antenna locations and the achieved degrees of freedom (DOF), which is defined as a measure of the maximum number of sources that can be concurrently estimated. The DOF in 1D arrays is upper bounded by the number of virtual lags in the second order difference coarray (SODC) [12].

In the literature, various 2D-DOA estimation algorithms were formulated based on the SODC [6], [13], [14], [15], [16], sum coarray, or a combination of both [2], [17]. Few references, however, have exploited higher-order difference coarrays (4th-order) [4], [18], [19], [20], [21]. Some DOA estimation algorithms require a hole-free URA in the coarray domain. Billboard arrays [22], 2D nested arrays [23], open-box arrays [24], partially open-box arrays [25], and

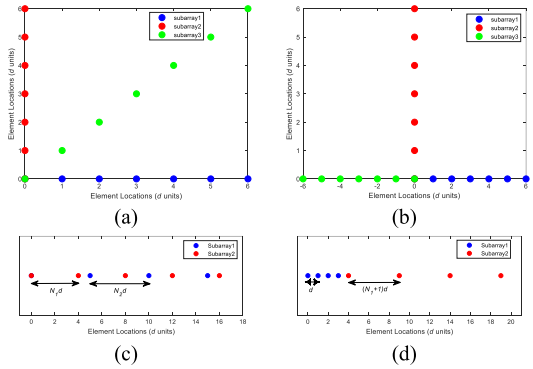

FIGURE 1. Sensor locations for (a) billboard (b) T-shaped arrays, (c) coprime array, and (d) nested array.

hourglass arrays [25] satisfy this property. If a coarray has missing virtual lag locations (holes), the DOF cannot be fully exploited. A comprehensive study for 2D antenna arrays can be found in [26]. The important L-shaped arrays can be modified by adding a third leg at 45° to form the billboard array as in Fig. 1(a) or by extending one leg to form the T-shaped array as in Fig. 1(b).

Joint polarization and 2D-DOA estimation algorithms were proposed using polarization sensitive array which consists of a co-centered orthogonal loop and dipole (COLD) sensors [27], [28], [29], [30]. The authors in [27], [28] proposed a parallel coprime array which can increase the DOF and improve the estimation accuracy. Four parallel sparse linear subarrays [30] and sparse nonuniform rectangular array (SNRA) were considered in [31]. The authors studied nested, coprime, and minimum redundancy sparse subarrays [30]. Other researchers used electromagnetic vector sensor (EMVS) [31], [32], [33]. A spatially spread acoustic vector sensor consisting of a tri-axial velocity vector sensor and an isotropic pressure sensor was examined in [34].

In this article, the L-shaped array is modified by adding a third leg either at 45° between the other two legs or along one of the legs, where three similar 1D sparse arrays are used. The candidate sparse arrays are the conventional coprime [35], rotated conventional nested [36], and super nested arrays [37]. The rotated T-shaped structure can be considered as a modified version of [21]. It has been shown that large DOF can be realized by exploiting the fourth-order difference coarray (FODC). In addition to extending the CRB for fourth order coarray, closed-form expressions for sensor locations and number of consecutive lags, or uniform-DOF (uDOF), in the FODC are derived for all arrays. The maximum DOF is achieved when the coprime pairs N_1 and N_2 are selected as close as possible. Additionally, the maximum DOF of nested and super nested based structures is achieved following the approach in [36]. All proposed configurations have better uDOF compared with hourglass array (HA) [25] and 2D nested planar array (2DNA) [23]. The proposed T-shaped nested array has comparable uDOF with the L-shaped nested array (ALNA) [20] which requires very large aperture size. The weight functions are also derived and investigated. The most significant weights have constant values irrespective of number of sensors, except for nested based structure. The HA has a hole-free difference coarray. However, the weight values are larger compared with the proposed configurations. The proposed arrays have promising performance for 2D-DOA estimation in the presence of mutual coupling compared with state of art.

The rest of the article is organized as follows: Section II introduces the structure of the proposed arrays. Section III presents the model for 2D-DOA estimation. Section IV explains the performance metrics used to evaluate the proposed arrays. Section V presents the derived Cramér-Rao bound (CRB). Section VI presents the results and discussions about the weight function, number of consecutive lags, and estimation accuracy. Finally, Section VII concludes the article.

II. PROPOSED ARRAY AND 2D-DOA MODELS

The developed arrays are derived from the prototype billboard and the T-shaped (rotated-T) arrays shown in Fig. 1(a) and (b), respectively. All ULAs are replaced with 1D sparse arrays at a time, including coprime array [35], nested array [36], and the super nested array [37].

A. BILLBOARD ARRAYS

The first sparse billboard design is achieved by replacing each subarray in Fig. 1(a) by the conventional coprime array [35]. Coprime arrays consist of two uniform linear subarrays having N_1 and N_2 elements, where N_1 and N_2 are two coprime integers, and $N_2 > N_1$. The elements of the subarray that has N_1 elements are spaced by $N_2 d$, while the elements of the subarray that has N_2 elements are spaced by $N_1 d$, with d being the minimum separation between any two elements which is set as half the wavelength $\frac{\lambda}{2}$. The sensor locations are given as the union of the two sets,

$$\mathbb{P}_c = \{ N_1 n_2 d \,|0 \le n_2 \le N_2 - 1\} \cup \{N_2 n_1 d|0 \le n_1 \le N_1 - 1\} \tag{1}$$

Coprime array has a total of $N_c = N_1 + N_2 - 1$ sensors (one sensor is shared between the subarrays). Fig. 1(c) shows an example of coprime array with $N_1 = 4$ and $N_2 = 5$. The set of the elements of the billboard array is

$$\mathbb{S}_B = \mathbb{G}_{\mathrm{x}} \cup \mathbb{G}_{\mathrm{y}} \cup \mathbb{G}_{\mathrm{xy}} \tag{2}$$

where

$$\mathbb{G}_{\mathrm{x}} = \{(nd, 0) \,|nd \in \mathfrak{g}\} \tag{3}$$

$$\mathbb{G}_{\mathrm{y}} = \{(0, nd) \,|nd \in \mathfrak{g}\} \tag{4}$$

$$\mathbb{G}_{\mathrm{xy}} = \{(nd, nd) \,|nd \in \mathfrak{g}\} \tag{5}$$

and the set $\mathfrak{g} = \mathbb{P}_c$ describes the linear array used to construct the 2D array. The total number of elements is $N = 3N_c - 2 = 3(N_1 + N_2 - 1) - 2$.

To generate the billboard nested array, the coprime array is replaced by the nested array introduced in [36]. The

conventional nested array consists of two collinearly placed subarrays with different interelement spacing. Assume that subarray1 has N_1 elements with interelement spacing of d. Subarray2 has N_2 elements, but with interelement spacing of $(N_1+1)d$. Sensor locations are given as follows

$$\mathbb{P}_n = \{n_1 d \,|0 \le n_1 \le N_1 - 1\} \cup \{(n_2 (N_1+1) - 1)\, d \,|1 \le n_2 \le N_2\} \tag{6}$$

Nested array has a total of $N_n = N_1 + N_2$ sensors. Fig. 1(d) shows an example of nested array with $N_1 = 4$ and $N_2 = 4$. The 2D billboard nested array is constructed in the same way using (2)–(5) by setting $\mathfrak{g} = \mathbb{P}_{rn}$, where $\mathbb{P}_{rn} = (N_2(N_1+1)-1)d - \mathbb{P}_n$. Note that the nested array is rotated by swapping the positions of the dense subarray and the sparse subarray to improve the DOF and reduce the mutual coupling. The total number of elements is $N = 3N_n - 2 = 3(N_1+N_2) - 2$.

The billboard super nested array is constructed using the super nested array introduced in [37]. Super nested array is a modified version of the nested array that significantly reduces mutual coupling by relocating some of the elements of the nested array. The super nested array is used to define the billboard super nested array as in (2)–(5) with $\mathfrak{g} = \mathbb{P}_{sn}$. Super nested array with N_s elements can be constructed with $N_1 \ge 4$ and $N_2 \ge 3$ [37]. Note that the definition of the set $\mathbb{P}_{sn}$ is eliminated for brevity, and interested readers are referred to [37]. Similar to the nested case, the total number of elements is $N = 3N_s - 2 = 3(N_1+N_2) - 2$, where N_s is the total number of sensors in the super nested array.

B. T-SHAPED ARRAYS

The T-shaped arrays are constructed using three sparse arrays similar to the billboard case, but the third subarray is located along the negative side of the x-axis, see Fig. 1(b). The set of elements in the T-shaped 2D array is given as

$$\mathbb{S}_T = \mathbb{G}_{\mathrm{x}} \cup \mathbb{G}_{\mathrm{y}} \cup \mathbb{G}_{-\mathrm{x}} \tag{7}$$

where $\mathbb{G}_{\mathrm{x}}$ and $\mathbb{G}_{\mathrm{y}}$ are as defined in (3) and (4), respectively, and:

$$\mathbb{G}_{-\mathrm{x}} = \{(-nd, 0) \,|nd \in \mathfrak{g}\} \tag{8}$$

To construct the T-shaped coprime, nested, and super nested arrays, both (7) and (8) are used with the set $\mathfrak{g}$ being equal to $\mathbb{P}_c$, $\mathbb{P}_{rn}$, and $\mathbb{P}_{sn}$, respectively. The total number of elements is the same as their counterparts using billboard structures.[1]

III. 2D-DOA ESTIMATION

Assume that K uncorrelated signal sources located in the far-field of the sensor array generate narrowband signals that impinge on a 2D array. The kth source has an azimuth angle $\theta_k \in [0, \pi]$ and an elevation angle $\phi_k \in [0, 2\pi]$. The received signal at the output of the array over T samples or snapshots can be expressed as

$$\mathbf{y}(t) = \mathbf{A}\left(\bar{\boldsymbol{\theta}}, \bar{\boldsymbol{\phi}}\right)\mathbf{s}(t) + \mathbf{n}(t), \; t = 1, 2, \ldots, T \tag{9}$$

where $\mathbf{y}(t) = [y_1(t),\, y_2(t), \ldots,\, y_N(t)]^T$, $\mathbf{n}(t) = [n_1(t), n_2(t), \ldots, n_N(t)]^T$ is white Gaussian noise with zero mean and uncorrelated with the transmitted signal, $\mathbf{s}(t) = [s_1(t), s_2(t), \ldots, s_K(t)]^T$, $[.]^T$ is the transpose operator, and $\mathbf{A}(\bar{\boldsymbol{\theta}}, \bar{\boldsymbol{\phi}}) = [\mathbf{a}(\bar{\theta}_1, \bar{\phi}_1), \mathbf{a}(\bar{\theta}_2, \bar{\phi}_2), \ldots, \mathbf{a}(\bar{\theta}_K, \bar{\phi}_K)]$ is the manifold matrix of size $N \times K$, with $\mathbf{a}_k(\bar{\theta}_k, \bar{\phi}_k)$ being a steering vector that has an element $(n_x, n_y) \in \mathbb{S}_B$ or $\mathbb{S}_T$ given by $e^{j2\pi(\bar{\theta}_k n_x + \bar{\phi}_k n_y)}$, where $\bar{\theta}_k = \frac{d}{\lambda}\sin\theta_k \cos\phi_k$ and $\bar{\phi}_i = \frac{d}{\lambda}\sin\theta_k \sin\phi_k$ are the normalized DOAs. The 2D-DOA estimation is based on the fourth-order cumulant. The fourth-order cumulant matrix is given as [38]:

$$\begin{aligned}\mathbf{C}_4 &= E\left\{\left(\mathbf{Y}\otimes\mathbf{Y}^*\right)\left(\mathbf{Y}\otimes\mathbf{Y}^*\right)^H\right\} \\ &\quad - E\left\{\left(\mathbf{Y}\otimes\mathbf{Y}^*\right)\right\} E\left\{\left(\mathbf{Y}\otimes\mathbf{Y}^*\right)^H\right\} \\ &\quad - E\left\{\mathbf{Y}\mathbf{Y}^H\right\}\otimes E\left\{\left(\mathbf{Y}\mathbf{Y}^H\right)^*\right\} \\ &= \left(\mathbf{A}\odot\mathbf{A}^*\right)\mathbf{C}_s\left(\mathbf{A}\odot\mathbf{A}^*\right)^H \\ &= \breve{\mathbf{A}}\mathbf{C}_s\breve{\mathbf{A}}^H\end{aligned} \tag{10}$$

where $[.]^*$ and $[.]^H$ represent the complex conjugate and Hermitian operators, respectively, $\breve{\mathbf{A}} = \mathbf{A}\odot\mathbf{A}^*$ with $\otimes$ and $\odot$ being the Kronecker product and Khatri-Rao product, $\breve{\mathbf{a}}(\bar{\theta}_k, \bar{\phi}_k) = \mathbf{a}(\bar{\theta}_k, \bar{\phi}_k)\otimes\mathbf{a}^*(\bar{\theta}_k, \bar{\phi}_k)$, $\breve{\mathbf{A}}$ and $\mathbf{Y} = [\mathbf{y}_1(t_1), \mathbf{y}_2(t_2), \ldots, \mathbf{y}_N(t_T)]$ are matrices of size $N^2 \times K$ and $N \times T$, respectively, and $\mathbf{C}_s = \mathrm{diag}[g_1, g_2, \ldots, g_K]$ is a diagonal matrix with $g_k = \mathcal{C}(s_k(t), s_k^*(t), s_k(t), s_k^*(t))$ being the kurtosis of the kth source signal and $\mathcal{C}(.)$ denotes the cumulants operator. Vectorizing $\mathbf{C}_4$ yields [18]:

$$\mathbf{c} = \mathrm{vec}\left(\mathbf{C}_4\right) = \bar{\mathbf{A}}\rho \tag{11}$$

where vec(.) is the vectorization operator which turns a matrix into a column vector, $\overline{\mathbf{A}} = \breve{\mathbf{A}}\odot\breve{\mathbf{A}}^*$ is a matrix of size $N^4 \times K$ and $\boldsymbol{\rho} = [g_1, \ldots, g_K]^T$. The new extended steering matrix, $\bar{\mathbf{A}}$, is a function of the FODC, which has a total of l_u unique lags (the number of unique entries in each column of $\bar{\mathbf{A}}$). Though, the number of consecutive lags generated by the FODC is $l_c < l_u$. The measurements associated with consecutive lags are extracted and sorted to form a new vector as:

$$\mathbf{r} = \mathbf{B}\rho \tag{12}$$

where $\mathbf{B}$ is a matrix of size $l_c \times K$, with $\mathbf{b}_i(\bar{\theta}_i, \bar{\phi}_i)$ being a steering vector that has an element $(n_x', n_y') \in \mathbb{U}_4$ given by $e^{j2\pi(\bar{\theta}_i n_x' + \bar{\phi}_i n_y')}$, $\mathbb{U}_4$ is the largest URA segment in the FODC [20], [39]. By considering the consecutive segment of virtual lags (largest symmetric URA around the origin [20], [39]), 2D-DOA estimation can be performed finally based on $\mathbf{r}$ using 2D unitary ESPRIT algorithm [40].

[1] A MATLAB code available in https://github.com/alawsh21/Sparse-Billboard-and-T-Shaped-Arrays-for-Two-Dimensional-Direction-of-Arrival-Estimation.git can be used to construct the proposed arrays for any arbitrary N.

TABLE 1. Number of Virtual Lags and Aperture

	Billboard			T-shaped		
	Coprime	Nested	Super	Coprime	Nested	Super
l_u	3,873	5,449	5,361	4,511	6,537	5,107
l_c	2,209	2,209	1,849	3,249	5,929	2,601
D	16×16	19×19	19×19	32×16	38×19	38×19

In the presence of mutual coupling, sensors are influenced by their neighboring elements, and (9) becomes $\mathbf{Y} = \mathbf{CA}(\bar{\theta}, \bar{\phi})\mathbf{S} + \mathbf{N}$, where $\mathbf{C}$ is the mutual coupling matrix modeled as in [25], [37]. This matrix can be approximated by a B-banded symmetric Toeplitz matrix depending on the separation between the elements as [41]:

$$\langle \mathbf{C} \rangle_{\mathbf{n}_1, \mathbf{n}_2} \begin{cases} c\|\mathbf{n}_1 - \mathbf{n}_2\|_2, & \|\mathbf{n}_1 - \mathbf{n}_2\|_2 \leq B \\ 0, & \text{otherwise} \end{cases} \tag{13}$$

where $\mathbf{n}_1, \mathbf{n}_2 \in \mathbb{S}$, $\|.\|_2$ is the l_2-norm of a vector, and $c_0, c_1, \ldots, c_B$ are the mutual coupling coefficients with $1 = c_0 > |c_1| > |c_{\sqrt{2}}| \ldots > |c_B| > |c_{B+1}| = 0$, where $|\frac{c_l}{c_k}| = \frac{l}{k}$ for $l,\ k > 0$ [2], [25], [37].

IV. PERFORMANCE MEASURES

This section presents some performance measures used to evaluate and compare the proposed arrays. This includes: the number of unique/consecutive lags in the FODC, the aperture size, and the weight function in general.

A. DEGREES OF FREEDOM AND DIFFERENCE COARRAY

When using 4th-order statistics for estimation, the number of unique elements in the FODC is directly related to the DOF, which is the maximum number of detectable uncorrelated sources. This is significant for algorithms that exploit all the elements in the difference coarray even if it is not hole-free. If the used algorithm requires continuous segment, then the number of consecutive lags is more significant.

Definition: Difference Coarray: Let a 2D array be specified by a set $\mathbb{S}$, the SODC, $\mathbb{D}$, is the difference between sensor positions as:

$$\mathbb{D} = \{\mathbf{n}_1 - \mathbf{n}_2 \mid \mathbf{n}_1, \mathbf{n}_2 \in \mathbb{S}\} \tag{14}$$

The FODC, $\mathbb{D}_4$, can be calculated by taking the differences again but between the virtual positions generated by the set $\mathbb{D}$ as:

$$\mathbb{D}_4 = \{\mathbf{p}_1 - \mathbf{p}_2 \mid \mathbf{p}_1, \mathbf{p}_2 \in \mathbb{D}\} \tag{15}$$

In other words, $\mathbf{p}_1 = \mathbf{n}_1 - \mathbf{n}_2$ and $\mathbf{p}_2 = \mathbf{n}_3 - \mathbf{n}_4$ for any arbitrary sensor locations $\mathbf{n}_1, \mathbf{n}_2, \mathbf{n}_3, \mathbf{n}_4 \in \mathbb{S}$. The 4th-order difference coarray can be rewritten as: $\mathbb{D}_4 = \mathbf{p}_1 - \mathbf{p}_2 = (\mathbf{n}_1 - \mathbf{n}_2) - (\mathbf{n}_3 - \mathbf{n}_4) = (\mathbf{n}_1 + \mathbf{n}_4) - (\mathbf{n}_2 + \mathbf{n}_3)$, or $\mathbb{D}_4 = (\mathbf{n}_4 - \mathbf{n}_2) + (\mathbf{n}_1 - \mathbf{n}_3)$. Therefore, the FODC is also equivalent to the difference coarray of the second order sum coarray or the sum coarray of the SODC. The number of unique lags, l_u, of the FODC is equal to the cardinality of $\mathbb{D}_4$, that is $l_u = |\mathbb{D}_4|$. On the other hand, the number of consecutive lags, l_c, is equal to the cardinality of $\mathbb{U}_4$, that is $l_c = |\mathbb{U}_4|$, where $\mathbb{U}_4$ is the largest URA segment in the FODC [20], [39]. The variables l_u and l_c are also known as the DOF and the uDOF [39]. An example is shown in Fig. 2 for the FODC for all proposed arrays, where $N_1 = 4$ and $N_2 = 5$ for coprime case, and $N_1 = N_2 = 4$ for both nested and super nested cases. Therefore, the total number of elements is $N = 22$. The red dots in Fig. 2 represent the virtual lag locations, while the blue triangles represent the physical locations of the elements.[2] Table 1 summarizes the number of virtual lags and the required apertures. The achievable uDOF of these configurations are examined in Section VI-B in terms of 2D-DOA estimation.

The objective is to find closed-form expressions for the maximum achievable uDOF. Let's consider first a 1D coprime. Its SODC has $2(N_1 + N_2) - 1$ consecutive lags in the range of $-(N_1 + N_2 - 1) : (N_1 + N_2 - 1)$ and $> N_1N_2$ unique lags. The holes affect the FODC, though the structure guarantees that the FODC realizes at least $-2(N_1 + N_2 - 1) : 2(N_1 + N_2 - 1) = 4(N_1 + N_2) - 3$ consecutive lags. In case of nested and super nested arrays, the SODC and the FODC have $-(N_1 + 1)N_2 + 1 : (N_1 + 1)N_2 - 1 = 2N_2(N_1 + 1) - 1$ and $-2(N_1 + 1)N_2 + 2 : 2(N_1 + 1)N_2 - 2 = 4N_2(N_1 + 1) - 3$ unique lags (all are consecutive), respectively.

Focusing only on one array along any axis, relating the example above to this discussion and considering the FODC, coprime array has 33 consecutive lags, while nested and super nested arrays have 77 consecutive lags. Now if there is another identical array along the negative side of the same axis, as in the T-shaped arrays, this number will be doubled. Finally, this number will be squared, $\mathcal{O}(.^2)$, if this happens across all axes. Actually, larger URA is expected to be generated due to the contribution between the utilized three sparse arrays to form the billboard or the T-shaped configurations.

Extensive analysis was conducted to derive closed-form expressions for the uDOF, l_c, of the proposed arrays. Understanding the underlying structures was incorporated to finalize the derivation. The resultant FODCs always have symmetric URA around the origin. Thus, the idea starts by finding the (x, y) coordinate of any virtual lag on one of the four corners within the resultant URA (generated by the FODC). Then an expression, X, is drafted for the coordinates for different cases of N_1 and N_2. This expression is confirmed by intensive simulation. After that, the expression is doubled and incremented by one to account for the zero axis, that is $2X + 1$. Finally,

[2] A MATLAB code available in https://github.com/alawsh21/Sparse-Billboard-and-T-Shaped-Arrays-for-Two-Dimensional-Direction-of-Arrival-Estimation.git is provided to construct the proposed arrays and generate the FODC for any arbitrary N.

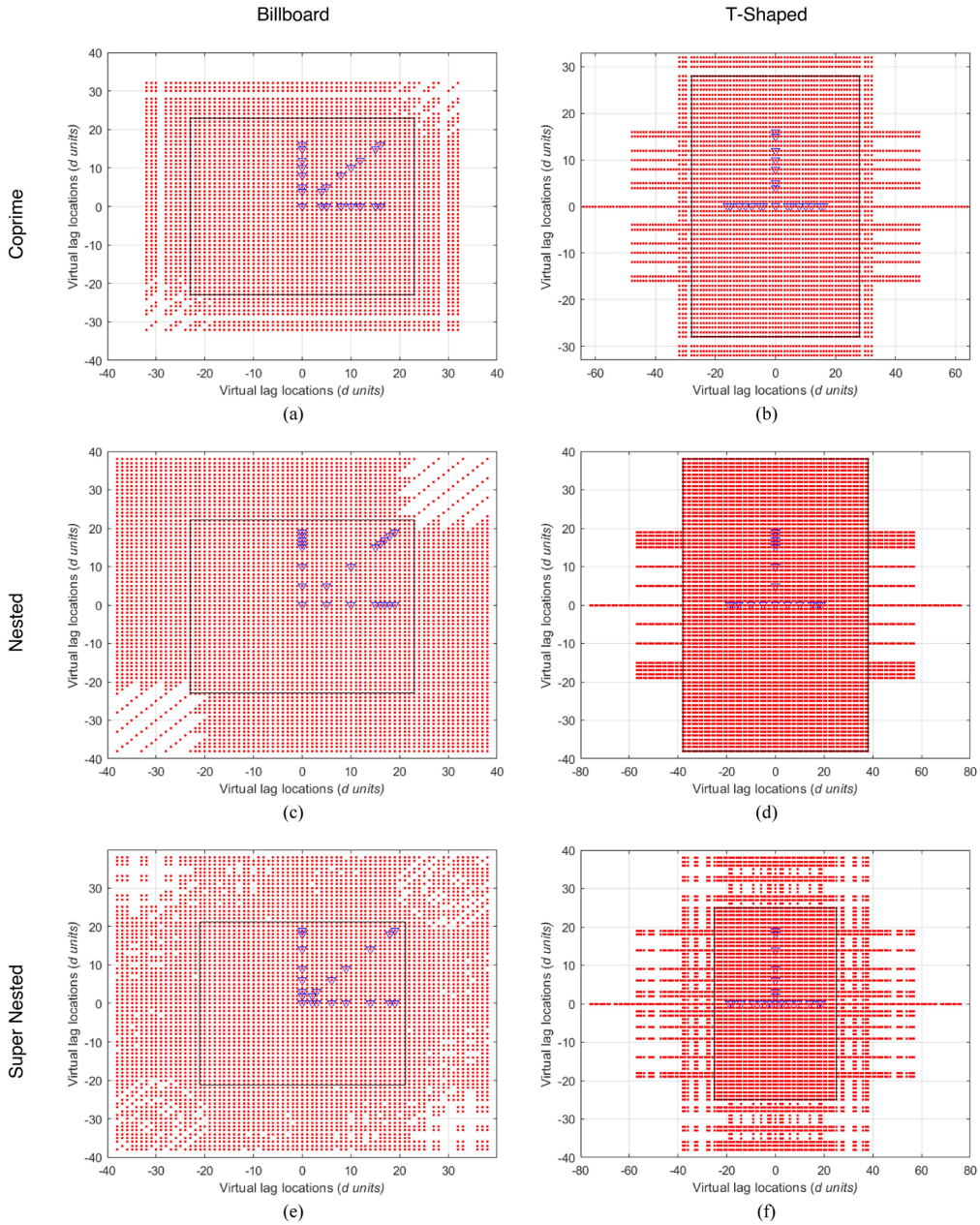

FIGURE 2. The FODC for (a), (c), (e) billboard-based arrays and (b), (d), (f) T-shaped-based arrays.

the result is squared to account for all consecutive lags as: $(2X+1)^2$.

Table 2 illustrates all closed-form expressions used to find the maximum achievable l_c or uDOF. Apart from super nested array, the formulas are applicable for arbitrary N_1 and N_2, provided that the greatest common divisor (GCD) is 1, i.e., $\text{GCD}(N_1, N_2) = 1$, and $N_2 > N_1$ for coprime case. The expressions related to super nested arrays are valid for the optimal selection of N_1 and N_2. [3]

When N_1 and N_2 are selected as close as possible in case of coprime, the maximum uDOF is achieved, similar to the 1D case [35]. Table 2 illustrates that the billboard coprime array has $\mathcal{O}(4N_2^4)$ uDOF, when $N_1 = N_2 - 1$, that is $2N_1 > N_2$. On the other hand, if we substitute $N_1 = N_2 - 1$ for $N_1 > 2$ (optimal selection) in the corresponding formula of the T-shaped coprime array from Table 2, we end up with $l_c = (2(N_2^2 + N_2) - 3)^2$. Therefore, the array has $\mathcal{O}(4(N_2^2 + N_2)^2)$

[3] A MATLAB code available in https://github.com/alawsh21/Sparse-Billboard-and-T-Shaped-Arrays-for-Two-Dimensional-Direction-of-Arrival-Estimation.git is developed to compare the derived and the simulated expressions for any arbitrary N.

TABLE 2. Derived Formulas for l_c Based on Billboard and T-Shaped

Shape	Configuration	uDOF	Condition
Billboard	Coprime	$(2(N_1N_2+N_1)-1)^2$	$2N_1 > N_2, N_1 > 2$
		$(2(N_1N_2-N_1+N_2)-1)^2$	$N_1 = 2, N_2 = 3$
			$2N_1 < N_2$
	Nested	$(2(N_1N_2+N_1+N_2)-1)^2$	$\forall N$
	Super Nested	$(2(N_1N_2+2N_1)-1)^2$	N_1, N_2: even, $\frac{N_1}{2}, \frac{N_2}{2}$: odd
		$\left(2\left(N_1N_2+\frac{3}{2}N_1\right)-1\right)^2$	$N_1, N_2, \frac{N_1}{2}, \frac{N_2}{2}$: even
		$(2(N_1N_2+N_2)+1)^2$	N_1, N_2: odd
			N_1: odd, $N_2, \frac{N_2}{2}$: even
			$N_1, \frac{N_2}{2}$: odd, N_2: even
		$\left(2\left(N_1N_2+\frac{3}{2}N_1\right)+1\right)^2$	$N_1, \frac{N_1}{2}$: even, N_2: odd
		$(2(N_1N_2+2N_1)+1)^2$	N_1: even, $\frac{N_1}{2}N_2$: odd
T-Shaped	Coprime	$(6N_2-1)^2$	$N_1 = 2$
		$(2(N_1N_2+N_1+N_2)-1)^2$	$N_1 > 2$
	Nested	$(4(N_1N_2+N_2)-3)^2$	$\forall N$
	Super Nested	$\left(2\left(N_1N_2+\frac{5}{2}N_1\right)-1\right)^2$	$N_1, N_2, \frac{N_1}{2}, \frac{N_2}{2}$: even
		$(2(N_1N_2+2N_1)+N_2)^2$	N_1, N_2: even, $\frac{N_1}{2}, \frac{N_2}{2}$: odd
			$N_1, \frac{N_1}{2}$: even, N_2: odd
		$(2(N_1N_2+2N_1)+N_2+2)^2$	N_1: even, $\frac{N_1}{2}N_2$: odd
		$(2(N_1N_2+2N_1+N_2)+1)^2$	N_1, N_2: odd
			N_1: odd, $N_2, \frac{N_2}{2}$: even
			$N_1, \frac{N_2}{2}$: odd, N_2: even

uDOF, which is larger than that of the billboard coprime array by $4N_2^2(2N_2+1)$.

The proposed nested and super nested arrays realize the maximum performance when N_1 and N_2 are selected as in the 1D case [36]. That is $N_1 = N_2 = \frac{N_n}{2}$ if N_n is even, whereas $N_1 = \frac{N_n-1}{2}$ and $N_2 = \frac{N_n+1}{2}$ if N_n is odd [36]. Remember that N_1 and N_2 are either equal or $N_2 = N_1 + 1$. This is also applicable for super nested array-based structures. Nested structures have one expression for any arbitrary N_1 and N_2, see Table 2. The billboard and T-shaped nested arrays realize $\mathcal{O}(\frac{1}{4}N_n^2(N_n+4)^2) = \mathcal{O}(\frac{4}{36^2}(N+2)^2(N+14)^2)$ uDOF and $\mathcal{O}(N_n^2(N_n+2)^2) = \mathcal{O}(\frac{1}{9^2}(N+2)^2(N+8)^2)$ uDOF, respectively.

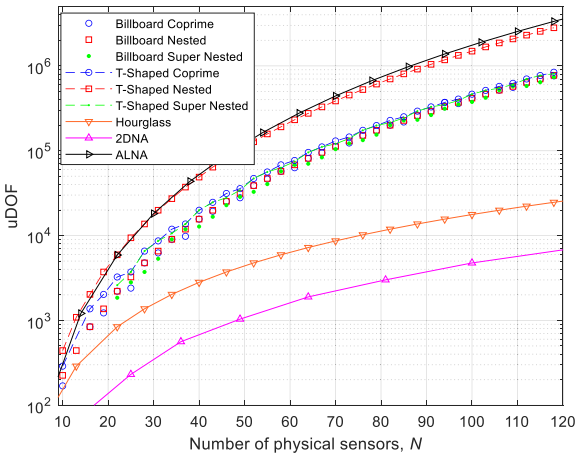

FIGURE 3. The uDOF or number of consecutive lags, l_c, versus N.

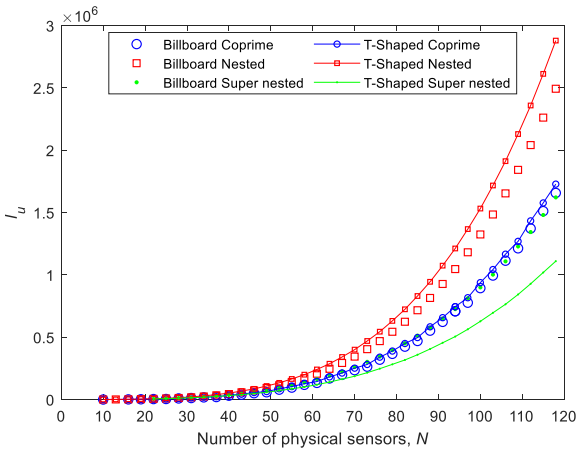

FIGURE 4. The number of unique lags, l_u, versus N.

There are different scenarios for super nested arrays, as indicated in Table 2. When N_1 is even and $\frac{N_1}{2}, N_2$ are both odd (N and N_s are both odd), for billboard case, $l_c = (2(N_1N_2+2N_1)+1)^2$ and the array attains $\mathcal{O}(\frac{1}{4}(N_s-1)^2(N_s+5)^2) = \mathcal{O}(\frac{1}{18^2}(N+2)^2(N+14)^2)$ uDOF. The T-shaped super nested array has $l_c = (2(N_1N_2+2N_1+N_2)+1)^2$, when N_1, N_2 : odd or N_1 : odd, $N_2, \frac{N_2}{2}$: even or $N_1, \frac{N_2}{2}$: odd, N_2 : even. The first condition implies even N_s and N, so $l_c = (\frac{1}{2}(N_s^2+6N_s)+1)^2$. While N_s and N are odd based on the other conditions, consequently $l_c = (\frac{1}{2}(N_s^2+6N_s)-5)^2$. These were achieved by replacing N_1 and N_2 by the optimal selection [36]. Super nested-based structures attain $\mathcal{O}(\frac{1}{18^2}(N+2)^2(N+20)^2)$ uDOF.

Considering the FODC, a comparison between the different billboard and T-shaped variants in terms of uDOF (l_c) and l_u, is illustrated in Figs. 3 and 4, respectively. The optimal conventional arrays are used for all configurations. Specifically,

N_1 and N_2 are selected as close as possible for coprime case [35] and $N_1 = N_2 = \frac{N_n}{2}$ or $N_1 = \frac{N_n-1}{2}$ and $N_2 = \frac{N_n+1}{2}$ if N_n is even or odd, respectively, for nested and super nested cases [36]. Super nested array can be constructed for $N_1 \geq 4$ and $N_2 \geq 3$ [37]. This is why the traces in Figs. 3 and 4 start from $N = 3N_s - 2 = 3(N_1 + N_2) - 2 = 22$ elements, where N_s is the number of sensors of the underlaying super nested array. In case of coprime ($N_1 = 2,\ N_2 = 3$) and nested ($N_1 = N_2 = 2$) based structures, it starts at $N = 10$ elements.

Fig. 3 shows the uDOF or number of consecutive lags versus the total number of elements, N, for all derived expressions in Table 2. All expressions were verified by simulation. The T-shaped nested array achieves the largest number of consecutive lags. The billboard coprime and nested structures achieve comparable performance. The T-shaped coprime and super nested structures achieve comparable performance. The billboard super nested array realizes the smallest number of consecutive lags among all configurations. Redistributing the elements of the dense array to reduce mutual coupling is the main reason. The uDOF, l_c, of the proposed configurations are compared with the HA [25], 2DNA [23], and ALNA [20] based on the FODC. All proposed configurations have better performance compared with HA and 2DNA, as demonstrated in Fig. 3. The ALNA and the T-shaped nested array have comparable uDOF.

The number of simulated unique lags, l_u, versus the total number of elements, N, are shown in Fig. 4. The T-shaped structures enjoy larger l_u compared with billboard, except for super nested array. The T-shaped nested array shows a clear superiority compared with others. This structure also enjoys few holes. Note how close are the two traces of nested case in Figs. 3 and 4. Though this is at the expense of mutual coupling and aperture size. The billboard coprime, super nested, and T-shaped coprime arrays achieve almost comparable performance. The billboard super nested array realizes the smallest number of consecutive lags among all configurations.

B. APERTURE SIZE

Due to the use of sparse arrays instead of ULAs in each leg, the proposed structures require larger aperture size than the already existing billboard and T-shaped arrays. This gives higher estimation accuracy but increases at the physical size and space requirements. Expressions for the aperture size are summarized in Table 3. Note that the aperture size of the T-shaped array is twice its counterpart using billboard structure. Nested and super nested structures have equal aperture.

The achieved uDOF is directly proportional to the aperture of the array. Large aperture size is considered a disadvantage when small form-factor is required. Fig. 5 shows the required aperture size for the considered 2D array configurations. Due to the introduced shift between the two nested subarrays, the ALNA, which has the largest uDOF, requires the largest aperture. The proposed T-shaped-based structures require larger aperture than billboard-based structures. HA and 2DNA have comparable apertures.

TABLE 3. Aperture Size

Array		Aperture (d units)
Billboard	Coprime	$N_1(N_2-1) \times N_1(N_2-1)$
	Nested	$(N_2(N_1+1)-1) \times (N_2(N_1+1)-1)$
	Super Nested	$(N_2(N_1+1)-1) \times (N_2(N_1+1)-1)$
T-Shaped	Coprime	$2N_1(N_2-1) \times N_1(N_2-1)$
	Nested	$2(N_2(N_1+1)-1) \times (N_2(N_1+1)-1)$
	Super Nested	$2(N_2(N_1+1)-1) \times (N_2(N_1+1)-1)$

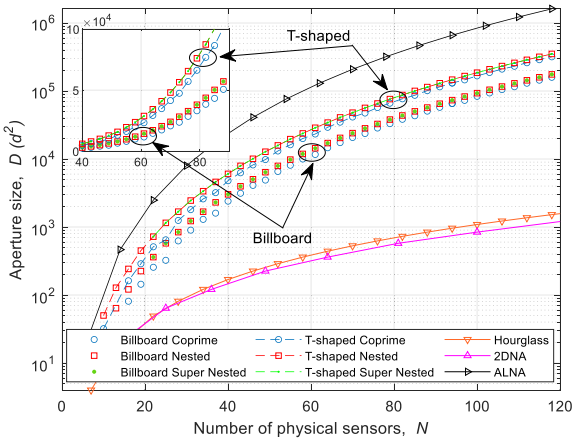

FIGURE 5. The required aperture size versus the total number of elements.

C. 2D WEIGHT FUNCTION

The weight function is a popular measure used to quantify the performance of antenna arrays for DOA estimation in the presence of mutual coupling. It is known that the closer the sensors are to each other, the more significant the effect of mutual coupling is. The definition of the weight function of the difference coarray for 2D arrays is given as

Definition: Weight Function of the Difference Coarray: Let a 2D array be specified by the set $\mathbb{S}$, and let its SODC be $\mathbb{D}$. The weight function of the difference coarray describes how many pairs of elements in $\mathbb{S}$ generate each element in $\mathbb{D}$. In other words, how many sensor pairs in $\mathbb{S}$ are separated by m_x and m_y in x and y directions, respectively, [25]:

$$w(\mathbf{m}) = |\{(\mathbf{n}_1, \mathbf{n}_2) \in \mathbb{S}^2 | \mathbf{n}_1 - \mathbf{n}_2 = \mathbf{m}\}| \tag{16}$$

where $|.|$ denotes the cardinality operation and $\mathbf{m} = (m_x, m_y)$ is a vector of two components. The most significant weights that affect mutual coupling are the smallest ones. Particularly, $w(0,\ 1)$, $w(1,\ 0)$, $w(1,\ 1)$, and $w(1,\ -1)$ are the most important [25]. Further discussion of the obtained values is available in the next section. In addition to increasing the distance between consecutive elements to reduce mutual coupling, the mutual impedance, which depends on the type of

antennas, must be properly calibrated and computed [41], [42], [43], [44], [45].

V. THE CRAMÉR-RAO BOUND FOR FOURTH ORDER COARRAY

Few researchers derived the CRB for second order coarray model [46], [47], [48]. In this section, we derive the Cramér-Rao bound (CRB) for 2D-DOA for the constructed 2D arrays based on the fourth order coarray. The parameter vector in (9) and (10) is defined as:

$$\boldsymbol{\eta} = \left[\bar{\theta}_1, \ldots, \bar{\theta}_K, \bar{\phi}_1, \ldots, \bar{\phi}_K\right]^T \tag{17}$$

The (m, n)-th element of the Fisher information matrix, **FIM**, is given by:

$$\mathbf{FIM}_{mn} = T\ \mathrm{tr}\left[\frac{\partial \mathbf{C}_4}{\partial \eta_m}\mathbf{C}_4^{-1}\frac{\partial \mathbf{C}_4}{\partial \eta_n}\mathbf{C}_4^{-1}\right] \tag{18}$$

where tr[.] denotes the trace of a matrix. Because $\mathrm{tr}(\mathbf{AB}) = \mathrm{vec}(\mathbf{A}^T)^T\mathrm{vec}(\mathbf{B})$ and $\mathrm{vec}(\mathbf{AXB}) = (\mathbf{B}^T \otimes \mathbf{A})\mathrm{vec}(\mathbf{X})$, the previous formula can be expressed as:

$$\mathbf{FIM}_{mn} = T\left[\frac{\partial \mathbf{c}}{\partial \eta_m}\right]^H \left(\mathbf{C}_4^T \otimes \mathbf{C}_4\right)^{-1}\frac{\partial \mathbf{c}}{\partial \eta_n} \tag{19}$$

with $\frac{\partial \mathbf{c}}{\partial \boldsymbol{\eta}}$ being the derivative of $\mathbf{c}$ with respect to $\boldsymbol{\eta}$ given as:

$$\frac{\partial \mathbf{c}}{\partial \boldsymbol{\eta}} = \left[\frac{\partial \mathbf{c}}{\partial \bar{\theta}_1} \cdots \frac{\partial \mathbf{c}}{\partial \bar{\theta}_K}\ \frac{\partial \mathbf{c}}{\partial \bar{\phi}_1} \cdots \frac{\partial \mathbf{c}}{\partial \bar{\phi}_K}\right] \tag{20}$$

As a matrix, the **FIM** can be further expressed as:

$$\mathbf{FIM} = T\left[\frac{\partial \mathbf{c}}{\partial \boldsymbol{\eta}}\right]^H \left(\mathbf{C}_4^T \otimes \mathbf{C}_4\right)^{-1}\frac{\partial \mathbf{c}}{\partial \boldsymbol{\eta}} \tag{21}$$

The derivatives in (20) can be calculated based on (11) as:

$$\frac{\partial \mathbf{c}}{\partial \boldsymbol{\eta}} = \left[\bar{\mathbf{A}}_{d\bar{\theta}}\mathbf{C}_s \quad \bar{\mathbf{A}}_{d\bar{\phi}}\mathbf{C}_s\ \right] \tag{22}$$

where $\bar{\mathbf{A}} = \breve{\mathbf{A}} \odot \breve{\mathbf{A}}^*$, $\breve{\mathbf{A}} = \mathbf{A} \odot \mathbf{A}^*$, $\bar{\mathbf{A}}_{d\bar{\theta}} = \breve{\mathbf{A}}_{d\bar{\theta}} \odot \breve{\mathbf{A}}^* + \breve{\mathbf{A}} \odot \breve{\mathbf{A}}_{d\bar{\theta}}^*$, $\bar{\mathbf{A}}_{d\bar{\phi}} = \breve{\mathbf{A}}_{d\bar{\phi}} \odot \breve{\mathbf{A}}^* + \breve{\mathbf{A}} \odot \breve{\mathbf{A}}_{d\bar{\phi}}^*$, $\breve{\mathbf{A}}_{d\bar{\theta}} = \mathbf{A}_{d\bar{\theta}} \odot \mathbf{A}^* + \mathbf{A} \odot \mathbf{A}_{d\bar{\theta}}^*$, $\breve{\mathbf{A}}_{d\bar{\phi}} = \mathbf{A}_{d\bar{\phi}} \odot \mathbf{A}^* + \mathbf{A} \odot \mathbf{A}_{d\bar{\phi}}^*$, and [46], [47]:

$$\mathbf{A}_{d\bar{\theta}} = \left[\frac{\partial \mathbf{a}\left(\bar{\theta}_1, \bar{\phi}_1\right)}{\partial \bar{\theta}_1}, \frac{\partial \mathbf{a}\left(\bar{\theta}_2, \bar{\phi}_2\right)}{\partial \bar{\theta}_2} \cdots \frac{\partial \mathbf{a}\left(\bar{\theta}_1, \bar{\phi}_1\right)}{\partial \bar{\theta}_K}\right] \tag{23}$$

$$\mathbf{A}_{d\bar{\phi}} = \left[\frac{\partial \mathbf{a}\left(\bar{\theta}_1, \bar{\phi}_1\right)}{\partial \bar{\phi}_1}, \frac{\partial \mathbf{a}\left(\bar{\theta}_2, \bar{\phi}_2\right)}{\partial \bar{\phi}_2} \cdots \frac{\partial \mathbf{a}\left(\bar{\theta}_1, \bar{\phi}_1\right)}{\partial \bar{\phi}_K}\right] \tag{24}$$

Here $\mathbf{C}_4$ and $\left(\mathbf{C}_4^T \otimes \mathbf{C}_4\right)^{-1}$ are positive definite, and its square root $\left(\mathbf{C}_4^T \otimes \mathbf{C}_4\right)^{-1/2}$ exists. Let's define $\mathbf{M} = [\mathbf{M}_{\bar{\theta}},\ \mathbf{M}_{\bar{\phi}}]$, with [46], [47]:

$$\begin{aligned}\mathbf{M}_{\bar{\theta}} &= \left(\mathbf{C}_4^T \otimes \mathbf{C}_4\right)^{-\frac{1}{2}}\mathbf{A}_{d\bar{\theta}}\mathbf{C}_s \\ \mathbf{M}_{\bar{\phi}} &= \left(\mathbf{C}_4^T \otimes \mathbf{C}_4\right)^{-\frac{1}{2}}\mathbf{A}_{d\bar{\phi}}\mathbf{C}_s\end{aligned} \tag{25}$$

Therefore, the **FIM** becomes $\mathbf{FIM} = T\mathbf{M}^H\mathbf{M}$. The CRB matrix for 2D-DOA is calculated by block-wise inversion as:

$$\mathrm{CRB}_{\eta_i} = [\mathbf{FIM}]_{ii} = \frac{1}{T}\left(\mathbf{M}^H\mathbf{M}\right)^{-1} \tag{26}$$

VI. RESULTS AND DISCUSSION

The performance results related to the weight function, 2D-DOA estimation, and CRB are discussed in this section.

A. THE WEIGHT FUNCTION

From mutual coupling perspective, the most significant weights in the 2D weight function are $w(0,\ 1)$, $w(1,\ 0)$, $w(1,\ 1)$, and $w(1,\ -1)$. Apart from nested-based structure, the proposed array structures offer significantly low values, see Table 4. Details on coprime based arrays and nested based arrays are presented, and then extended to super nested configurations.

1) BILLBOARD COPRIME ARRAY

For billboard coprime array, the weight $w(1,\ 0)$ describes the number of elements spaced by 1 in x and 0 in y. The minimum spacing in the cross differences between any two legs is N_1, which is greater than 1. Therefore, we are only left with the self-differences of the leg that lays on the x-axis. It was proved in [49] that a 1D coprime array has only two pairs of sensors separated by d, i.e., $w(1,\ 0) = 2$. The same argument holds true for the case of $w(0,\ 1)$. However, this time, the only contribution to this weight is from the self-differences generated by the y-axis leg. Therefore, $w(0,\ 1) = 2$.

To have a separation of 1 in x and y, $w(1,\ 1)$, the cross differences are all eliminated because the minimum separation between any two legs is N_1. Moreover, the self-differences of the legs laying on the x and y axes are eliminated as well, because they have either the same x or y coordinates. The only contribution left is from the self-differences of the third leg that lays on the $x = y$ straight line. The elements in this leg have equal x and y coordinates. Therefore, if we consider each coordinate separately, we can use the fact for the 1D coprime array to show that this leg has 2 pairs of elements separated by d in x and y. Hence, $w(1,\ 1) = 2$ and the overall spacing between the two elements is $\sqrt{2}d$.

Regarding $w(1,\ -1)$, consider two elements and assume that the first element has less x coordinate value than the second element. The y coordinate of the first element must be greater than that of the second element to be counted in this weight. However, this is impossible; because as you increase x, y either increases, or stays unchanged, thus, $w(1,\ -1) = 0$.

2) T-SHAPED COPRIME ARRAY

To explain the result, consider the weight $w(1,\ 0)$, the elements that generate this weight must have the same y coordinate. This is not possible except for elements on the x-axis. Therefore, the part of the array that lays on the y-axis does not contribute to this weight. Furthermore, we can eliminate the cross differences generated from the two legs that lay

TABLE 4. 2D Weight Function Values

Structures			Weight Functions			
			$w(1,0)$	$w(0,1)$	$w(1,1)$	$w(1,-1)$
Billboard	Coprime		2	2	2	0
	Nested		N_1	N_1	N_1	0
	Super nested	Odd N_1	1	1	1	0
		Even N_1	2	2	2	0
T-shaped	Coprime		4	2	0	0
	Nested		$2N_1$	N_1	0	0
	Super nested	Odd N_1	2	1	0	0
		Even N_1	4	2	0	0
Hourglass [25]*			2	{8 or 10}*	{3,5,7, or 9}*	{3,5,7, or 9}*
2DNA [23]**			$(N_{dx}+N_{sx})N_{dx}$	$(N_{dy}+N_{sy})N_{dy}$	$N_{dx}N_{dy}$	$N_{dx}N_{dy}$
ALNA [20]***			N_{x1}	N_{y1}	0	0

* refer to [25] for details.
** N_{dx}, N_{sx} (N_{dy}, N_{sy}) denote the number of elements in the dense and sparse subarrays along x-axis (y-axis), respectively.
*** N_{x1} and N_{y1} denote the number of elements in the dense subarrays along x and y axes respectively.

on the x-axis; because the minimum distance between the two legs that lay on the positive and negative x-axis, is N_1 which is greater than 1. What is left now to contribute to this weight are the self-differences generated by each leg in the x-axis. It was proved in [49] that a 1D coprime array has only two pairs of sensors separated by d. Therefore, each leg on the x-axis will have 2 elements separated by $(1,\ 0)$ and the whole 2D array will have $w(1,\ 0) = 4$.

The same argument can be used for $w(0,\ 1)$. This time, the elements present on the x-axis do not contribute to the weight. Therefore, the only contribution is due to the leg that lays on the y-axis which results in a value of 2 for this weight, $w(0,\ 1) = 2$. For $w(1,\ 1)$, all elements in the T-shaped structure are either placed in the x or y axes. Moreover, the minimum distance between any two legs is N_1 which is greater than 1. Therefore, $w(1,\ 1) = 0$. Regarding $w(1,\ -1)$, a single leg cannot generate this weight because all legs lay on either x-axis or y-axis. Furthermore, the minimum distance between any two legs is $N_1 > 1$. Therefore, $w(1,\ -1) = 0$.

3) BILLBOARD NESTED ARRAY

For the billboard nested array, the important values for the weight function are summarized in Table 4. Only the self-differences generated from the elements within the dense subarray along the x-axis (subarray 1) contribute to $w(1,\ 0)$, because the elements should have equal y coordinates. So $w(1,\ 0) = N_1$. Similarly, $w(0,\ 1) = N_1$. The self-differences generated form subarray 3 contribute to $w(1,\ 1) = N_1$. All self-differences generated from the three subarrays don't contribute to $w(1,\ -1)$. This is because when the elements are separated by 1 in the x coordinates, they will be separated by 0 or 1 when subarray 1 or subarray 3 are considered, respectively. In addition, separation by 1 in y coordinates implies 0 separation in x coordinates in case of subarray 2, so $w(1,\ -1) = 0$. The cross-differences don't contribute to any of these weights because the minimum spacing between the closest two elements in the three subarrays is $(N_1 + 1) > 1$.

4) T-SHAPED NESTED ARRAY

For the T-shaped nested array, only the self-differences generated from the elements within the dense subarrays along the x-axis (subarray 1 & 3) contribute to $w(1,\ 0)$, because the elements should have equal y coordinates. As a result, $w(1,\ 0) = 2N_1$, and similarly $w(0,\ 1) = N_1$. The other two weights $w(1,\ 1) = w(1,\ -1) = 0$ can be proved based on $w(1,\ 0)$ or $w(0,\ 1)$. If two elements are separated by 1 in x coordinates, then their separation in y coordinates become 0, not 1 or -1, and vice-versa. The cross-differences don't contribute to any of them because the minimum spacing between the closest two elements in the three subarrays is $(N_1 + 1) > 1$.

The discussion can be extended to the arrays based on the 1D super nested array. The 1D super nested array has different weights for odd and even values of N_1 [37], that is for odd N_1, $w(1) = 1$, and for even N_1, $w(1) = 2$. The obtained values for the coprime, nested, and super nested based arrays are presented in Table 4. Note that the nested array-based structures do not possess small or constant values for the weight functions due to the presence of the dense ULA segment in each leg.

The self-differences of each leg have a direct impact on $w(0,\ 1)$, $w(1,\ 0)$, $w(1,\ 1)$, and $w(1,\ -1)$, if $\mathbf{n}_2 - \mathbf{n}_1 > 1$, where $\mathbf{n}_1$ and $\mathbf{n}_2$ are the locations of the first and second elements in each 1D subarray, respectively. In other words, the separation of the first two elements in each leg is greater than d. Using this, we can write the discussed weights as:

- Billboard

$$w\,(1,\ 0)=n,\ \ w\,(0,1)=n,\ w\,(1,\ 1)=n,\ w\,(1,\ -1)=0$$

- T-shaped

$$w\,(1,\ 0)=2n,\ w\,(0,1)=n,\ w\,(1,\ 1)=0,\ w\,(1,\ -1)=0$$

where n is the number of sensor pairs with a unit separation in the 1D leg.

The values are compared to those achieved by the hourglass array [25], 2DNA [23], and ALNA [20]. Apart from nested

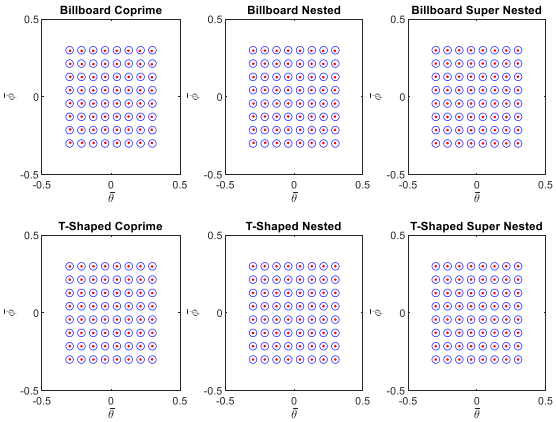

FIGURE 6. The true source directions (in circles) and the estimated directions (in dots) for billboard (upper) and T-shaped (lower) structures with noise free, no mutual coupling, and $T = 500$ samples.

based structures, the proposed arrays always have smaller weights except for $w(1,\ 0)$. Due to the dense subarrays, the 2DNA and ALNA have large weight functions, which increase linearly with the number of elements in the dense subarrays. The HA has larger weights compared with the proposed configurations, see Table 4.

B. PERFORMANCE IN DOA ESTIMATION

This subsection presents 2D-DOA estimation based on the FODC with 2D unitary ESPRIT algorithm [40]. To carry out the estimation, only the central URA, $\mathbb{U}_4$, contiguous part of $\mathbb{D}_4$ is utilized by ESPRIT. The number of snapshots is $T = 500$ and the SNR $=$ 0dB. A total of $K = 4$ uncorrelated sources are assumed and their normalized direction-cosines are equally-spaced as in [25] but without any rotation. The configurations presented in Section IV-A are assumed where the total number of elements of each array is $N = 22$, with $N_1 = 4$ and $N_2 = 5$ for coprime, and $N_1 = N_2 = 4$ for nested and super nested based structures. The mutual coupling parameters are $c_1 = 0.3$, $B = 5$, and $c_l = \frac{c_1}{l} e^{j\pi(l-1)/4}$ [25]. The root-mean-squared error (RMSE) is used to assess the performance, which combines both azimuth and elevation as:

$$\text{RMSE} = \sqrt{\frac{1}{IK} \sum_{i=1}^{I} \sum_{k=1}^{K} \left(\bar{\theta}_k - \widehat{\bar{\theta}}_k(i)\right)^2 + \left(\bar{\phi}_k - \widehat{\bar{\phi}}_k(i)\right)^2} \tag{27}$$

where $\widehat{\bar{\theta}}_k(i)$ and $\widehat{\bar{\phi}}_k(j)$ are the estimate of $\bar{\theta}_k$ and $\bar{\phi}_k$, respectively, at the i^{th} Monte Carlo trial, $i = 1,\ 2, \ldots, I$, and K is the number of sources to be localized. A total of $I = 100$ Monte-Carlo trials are used. All these parameters are fixed unless otherwise stated.

To examine the achievable DOF, a total of $K = 64$ sources are assumed in noise free environment and in the absence of mutual coupling. Fig. 6 shows the actual and the estimated cosine-directions marked in circles and dots, respectively. Due to the large uDOF (see Table 1), all arrays resolve all sources correctly. Note that the number of sources is larger than the number of sensors, $K > N$.

Fig. 7 shows the RMSE of the estimated DOAs for the proposed arrays ignoring the effect of mutual coupling when $K = 4$ sources. The RMSE is calculated when varying the SNR and keeping the number of snapshots as 500 in (a) and varying the number of snapshots and keeping the SNR as 0dB in (b). Hourglass array [25] is simulated using $N = 22$ elements, with $N_x = N_y = 8$. This array has a hole-free SODC and has excellent performance in the presence of mutual coupling. For fair comparison with hourglass array, the FODC is considered which is also a hole-free coarray. The coarray has $l_u = l_c = 841$ lags and the array requires $7d \times 7d$ aperture size. It is evident that the performance improves with the increase of SNR and number of samples. Due to their large uDOF, the T-shaped structures realize smaller RMSE at high SNR when mutual coupling is ignored. All proposed arrays attain smaller RMSE compared with hourglass array. Though, the latter requires smaller aperture size.

The effect of mutual coupling is considered in Fig. 8. Arrays based on the coprime and super nested arrays show more robustness against mutual coupling as expected due to their sparseness, except the billboard super nested array. The latter has small uDOF as Table 1 depicts. As per the weights presented in Table 4, the T-shaped super nested array has the smallest RMSE. Although the T-shaped nested array has the largest uDOF (see Table 1), mutual coupling deteriorates the performance. Above 0dB and around 300 samples, mutual coupling becomes dominant, and the performance does not improve.

Since K is small, the impact of mutual coupling is not significant. Increasing the number of sources makes the mutual coupling effect clear and deteriorates the estimation capability of some arrays, despite the large number of consecutive lags. Although 2D sparse arrays may estimate $K > N$ sources (see Fig. 6), the effect of mutual coupling makes the estimation process more challenging.

Fig. 9 shows how the RMSE depends on c_1, the most significant coefficient in mutual coupling model, when SNR $=$ 0 dB, $T = 500$ samples, and $K = 4$ sources. It can be concluded that the RMSE is small when c_1 is close to zero. The performance degrades above certain thresholds of c_1. These thresholds are the approximate values of c_1 at which the arrays can perform well in the presence of mutual coupling. Fig. 9 illustrates that the thresholds for the billboard-based structure are around 0.4 for coprime, 0.35 for nested, and 0.5 for super nested. This indicates that billboard super nested array is more robust to mutual coupling effects than others. Note that this array has also smaller uDOF as illustrated in Table 1. While the thresholds for the T-shaped based structure are around 0.65 for coprime, 0.8 for nested, and 0.75 super nested. Although nested based-structures have large mutual coupling, the large uDOF (see Table 1) contributes more to the performance. Note that the T-shaped based structures realize larger uDOF and have larger aperture size. Compared with state of art, the threshold is around 0.55 for hourglass array. Generally speaking and for the considered arrays, the T-shaped based structure is more robust to mutual coupling effects, where

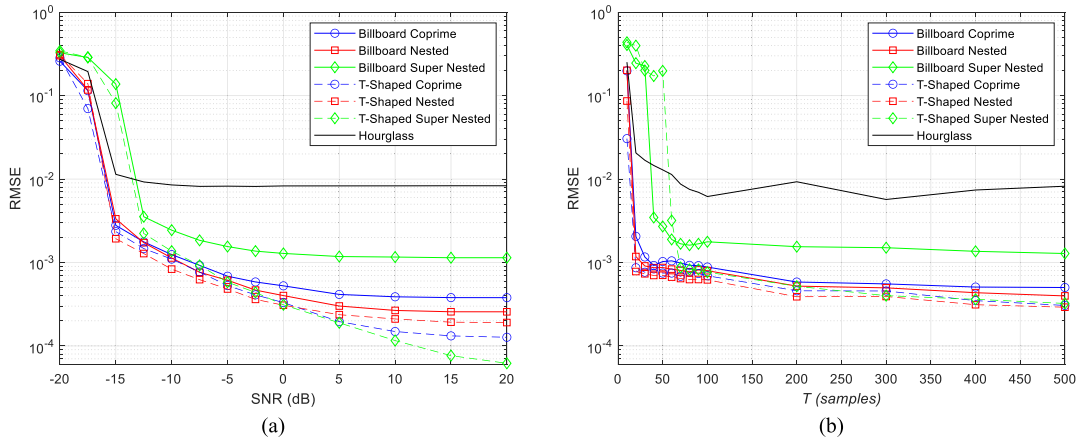

FIGURE 7. RMSE without mutual coupling versus (a) SNR (snapshots = 500) and (b) snapshots (SNR = 0 dB) for $K = 4$ sources.

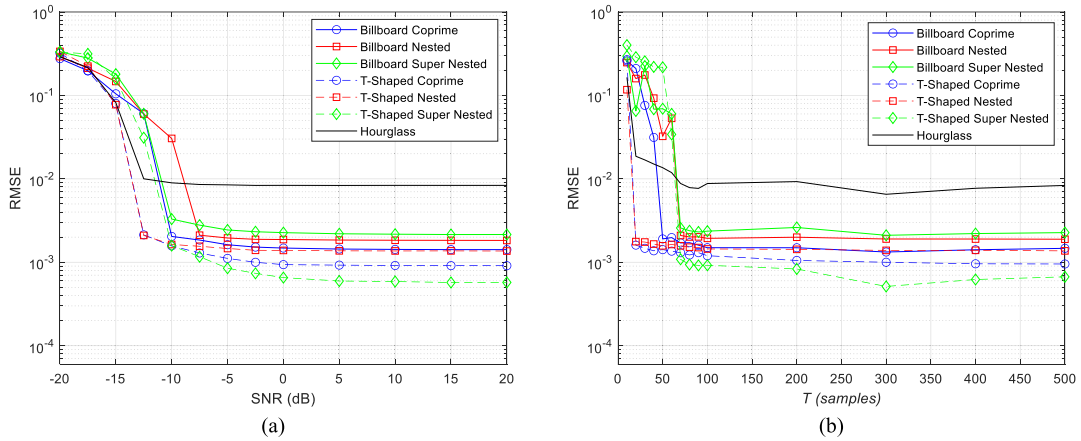

FIGURE 8. RMSE with mutual coupling versus (a) SNR ($T = 500$ samples) and (b) snapshots (SNR = 0 dB) for $K = 4$ sources.

TABLE 5. Arrays of Comparable UDOF With the Required Elements

	Billboard			T-shaped		
	Coprime	Nested	Super	Coprime	Nested	Super
l_c	19,321	**19,881**	22,801	**19,881**	**19,881**	**19,881**
N_1	7	7	8	7	5	7
N_2	9	8	8	8	6	7
N	43	43	46	40	31	40

TABLE 6. Average Running Time (SEC)

Arrays	Billboard			T-Shaped		
	Coprime	Nested	Super nested	Coprime	Nested	Super nested
Time (Sec)	0.7003	0.6832	0.6338	0.9593	2.0803	0.7636

$w(1,\ 0) = 4,\ w(0,\ 1) = 2,\ w(1,\ 1) = 0,\ w(1, -1) = 0$ for coprime and super nested.

In the previous scenarios, the total number of elements is the same for all configurations. Configurations with comparable number of consecutive lags are further evaluated. Table 5 demonstrates that the closest billboard super nested array has large uDOF. All arrays require comparable number of elements, except the T-shaped nested array. In the presence of mutual coupling, Fig. 10 shows the RMSE versus SNR with $K = 25$ sources. Due to the mutual coupling effect, nested structures have the worst RMSE, while the best performance is realized by super nested arrays.

The running time for all configurations is calculated for the scenarios in Fig. 7(a). The execution time over MATLAB was calculated on a PC with an AMD Ryzen 7 5700G processor with Radeon Graphics and 16 GB RAM at $\sim$ 3.8 GHz. The averaged running time in seconds is presented in Table 6. The T-shaped nested and billboard super nested arrays require the largest and the smallest running time for estimation, respectively. The running time is proportional to the uDOF as presented in Table 1.

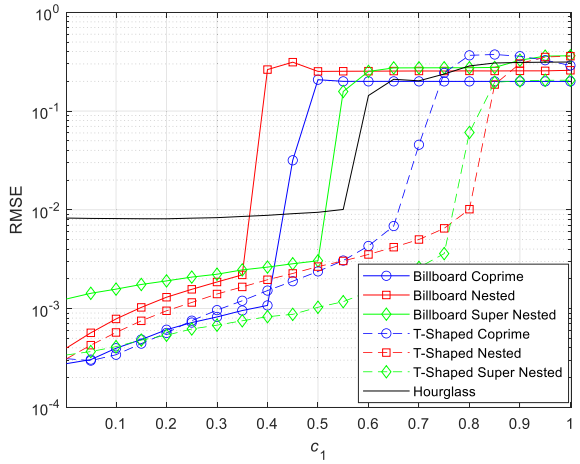

FIGURE 9. RMSE versus mutual coupling at SNR = 0 dB, $T = 500$ samples, and $K = 4$ sources.

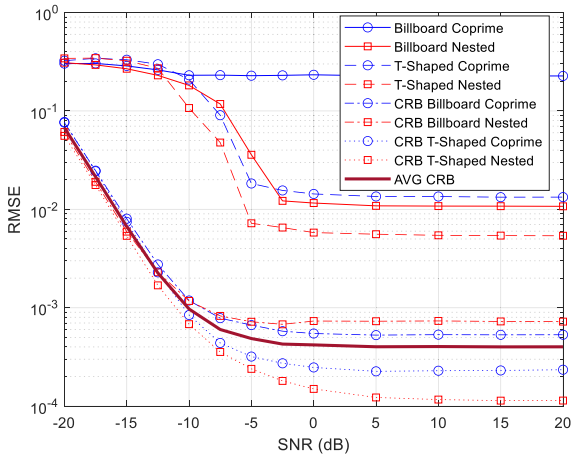

FIGURE 11. RMSE vs SNR with mutual coupling with $T = 500$ samples, $K = 4$ sources, and $N = 10$ elements.

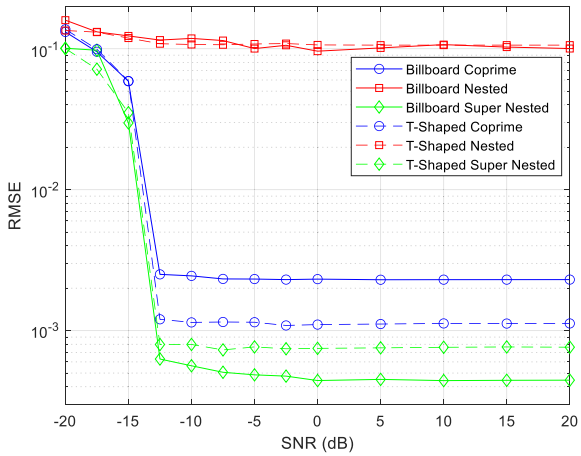

FIGURE 10. RMSE vs SNR with mutual coupling with $T = 500$ samples and $K = 25$ sources.

C. CRB FOR FOURTH ORDER COARRAY

The derived CRB of the proposed configurations requires very high computation. The size of the term $\mathbf{C}_4^T \otimes \mathbf{C}_4$ in (25) is $N^4 \times N^4$. Consequently, this cannot be easily handled. To present the CRB, the total number of elements is reduced from $N = 22$ to $N = 10$. The billboard and T-shaped super nested arrays cannot be constructed because the minimum values are $N_1 \geq 4$ and $N_2 \geq 3$ [37]. Coprime and nested arrays with $N_1 = 2,\ N_2 = 3$ and $N_1 = 2,\ N_2 = 2$ are assumed. Fig. 11 shows the RMSE with mutual coupling versus SNR when $T = 500$ samples, $K = 4$ sources, and $N = 10$ elements. The selected parameters lead to equal weight values for the considered configurations. Due to their large aperture and uDOF, nested based structures have small RMSEs. Billboard coprime array has poor performance due to the small uDOF. The CRBs for the four considered arrays, included based on (26), are comparable. Even when configurations have equal FODC, their CRBs are not the same because the CRB depends on the sensor locations [50].

VII. CONCLUSION

In this article, we examined six 2D arrays derived from the billboard and T-shaped arrays. Each 2D array is constructed using three identical 1D sparse arrays; namely, coprime, nested, and super nested arrays. The proposed arrays achieve large DOF when the FODC is exploited. They also enjoy closed-form sensor locations, and have closed formulas for the number of consecutive lags. The T-shaped structures result in a higher DOF compared with the billboard structure. Among the six arrays, the four arrays based on coprime and super nested arrays offer significantly reduced values for the smallest weights in the 2D weight function of the difference coarray. Simulation results confirmed the robustness of the proposed arrays in the presence of mutual coupling.

REFERENCES

[1] H. L. van Trees, *Optimum Array Processing: Part IV of Detection, Estimation, and Modulation*. Hoboken, NJ, USA: Wiley, 2002.

[2] X. Li, X. Wang, W. Wang, and S. Ren, "Generalized L-shaped array based on the difference and sum coarray concept," *IEEE Access*, vol. 8, pp. 140456–140466, 2020, doi: 10.1109/access.2020.3012527.

[3] Z. Zhang, Y. Guo, Y. Huang, and P. Zhang, "A 2-D DOA estimation method with reduced complexity in unfolded coprime L-shaped array," *IEEE Syst. J.*, vol. 15, no. 1, pp. 407–410, Mar. 2019, doi: 10.1109/jsyst.2019.2948089.

[4] X. Wu and J. Yan, "3-D mixed far-field and near-field sources localization with cross array," *IEEE Trans. Veh. Technol.*, vol. 69, no. 6, pp. 6833–6837, Jun. 2020.

[5] Y. Hua, T. K. Sarkar, and D. Weiner, "An L-shaped array for estimating 2-D directions of wave arrival," *IEEE Trans. Antennas Propag.*, vol. 39, no. 2, pp. 143–146, Feb. 1991, doi: 10.1109/mwscas.1989.101873.

[6] F. Wu, F. Cao, X. Ni, C. Chen, Y. Zhang, and J. Xu, "L-shaped sparse array structure for 2-D DOA estimation," *IEEE Access*, vol. 8, pp. 140030–140037, 2020, doi: 10.1109/access.2020.3012685.

[7] Y. Yang, X. Mao, Y. Hou, and G. Jiang, "2-D DOA estimation via correlation matrix reconstruction for nested L-shaped array," *Digit. Signal Process.*, vol. 98, 2020, Art. no. 102623, doi: 10.1016/j.dsp.2019.102623.

[8] H. A. L. I. Mirza, M. Asif, Z. Raja, N. I. Chaudhary, and I. M. Qureshi, "A robust multi sample compressive sensing technique for DOA estimation using sparse antenna array," *IEEE Access*, vol. 8, pp. 140848–140861, 2020, doi: 10.1109/ACCESS.2020.3011597.

[9] A. M. Elbir, "L-shaped coprime array structures for DOA estimation," *Multidimensional Syst. Signal Process.*, vol. 31, no. 1, pp. 205–219, 2020, doi: 10.1007/s11045-019-00657-4.

[10] Q. Liu, X. Yi, L. Jin, and W. Chen, "Two dimensional direction of arrival estimation for co-prime L-shaped array using sparse reconstruction," in *Proc. 8th Int. Congr. Image Signal Process.*, 2016, pp. 1499–1503.

[11] Y. Yang, Z. Zheng, H. Yang, J. Yang, and Y. Ge, "A novel 2-D DOA estimation method via sparse L-shaped array," in *Proc. IEEE 2nd Int. Conf. Comput. Commun.*, 2017, pp. 1865–1869.

[12] S. Qin, Y. D. Zhang, and M. G. Amin, "Generalized coprime array configurations for direction-of-arrival estimation," *IEEE Trans. Signal Process.*, vol. 63, no. 6, pp. 1377–1390, Mar. 2015.

[13] F. Sun, S. Ouyang, P. Lan, and F. Li, "Reduced dimensional 2-D DOA estimation via least partial search with automatic pairing for parallel co-prime arrays," in *Proc. IEEE 11th Sensor Array Multichannel Signal Process. Workshop*, 2020, pp. 1–5.

[14] S. Qin, Y. D. Zhang, and M. G. Amin, "Improved two-dimensional DOA estimation using parallel coprime arrays," *Signal Process.*, vol. 172, pp. 1–9, 2020, doi: 10.1016/j.sigpro.2019.107428.

[15] W. Si, F. Zeng, Z. Qu, and Z. Peng, "Two-dimensional DOA estimation via a novel sparse array consisting of coprime and nested subarrays," *IEEE Commun. Lett.*, vol. 24, no. 6, pp. 1266–1270, Jun. 2020.

[16] W. Zhang, Q. Wang, J. Huang, and N. Yuan, "Two-dimensional underdetermined DOA estimation of quasi-stationary signals via sparse Bayesian learning," *Radioengineering*, vol. 28, no. 3, pp. 627–634, 2019, doi: 10.13164/re.2019.0627.

[17] G. Wang, Z. Fei, S. Ren, and X. Li, "Improved 2D coprime array structure with the difference and sum coarray concept," *Electronics*, vol. 9, no. 2, pp. 1–25, 2020, doi: 10.3390/electronics9020273.

[18] J. He, L. Li, and T. Shu, "2-D direction finding using parallel nested arrays with full co-array aperture extension," *Signal Process.*, vol. 178, pp. 1–6, 2021, doi: 10.1016/j.sigpro.2020.107795.

[19] A. M. Molaei and M. Hoseinzade, "High-performance 2D DOA estimation and 3D localization for mixed near/far-field sources using fourth-order spatiotemporal algorithm," *Digit. Signal Process.*, vol. 100, 2020, Art. no. 102696, doi: 10.1016/j.dsp.2020.102696.

[20] X. Li, S. Ren, J. Liu, and W. Wang, "Augmented L-shaped nested array based on the fourth-order difference co-array concept," in *Proc. IEEE 10th Sensor Array Multichannel Signal Process. Workshop*, 2018, pp. 31–35.

[21] S. Liu, L. S. Yang, D. C. Wu, and J. H. Huang, "Two-dimensional DOA estimation using a co-prime symmetric cross array," *Prog. Electromagn. Res. C*, vol. 54, pp. 67–74, 2014.

[22] C. R. Greene and R. C. Wood, "Sparse array performance," *J. Acoust. Soc. Amer.*, vol. 61, no. 6, pp. 1866–1872, 1978.

[23] P. Pal and P. P. Vaidyanathan, "Nested arrays in two dimensions, Part I: Geometrical considerations," *IEEE Trans. Signal Process.*, vol. 60, no. 9, pp. 4694–4705, Sep. 2012, doi: 10.1109/TSP.2012.2203815.

[24] R. A. Haubrich, "Array design," *Bull. Seismological Soc. Amer.*, vol. 58, no. 3, pp. 111–151, 1968.

[25] C.-L. Liu and P. P. Vaidyanathan, "Hourglass arrays and other novel 2-D sparse arrays with reduced mutual coupling," *IEEE Trans. Signal Process.*, vol. 65, no. 13, pp. 3369–3383, Jul. 2017, doi: 10.1109/TSP.2017.2690390.

[26] I. Aboumahmoud, A. Muqaibel, M. Alhassoun, and S. Alawsh, "A review of sparse sensor arrays for two- dimensional direction-of-arrival estimation," *IEEE Access*, vol. 9, pp. 92999–93017, 2021, doi: 10.1109/ACCESS.2021.3092529.

[27] C. Hou, C. Fang, Z. Deng, Y. Wang, and W. Si, "Two-dimensional direction-of-arrival and polarization parameter estimation using parallel co-prime polarization sensitive array," *IEEE Access*, vol. 8, pp. 6566–6574, 2020, doi: 10.1109/ACCESS.2019.2957546.

[28] W. Si, Y. Wang, and C. Zhang, "Three-parallel co-prime polarization sensitive array for 2-D DOA and polarization estimation via sparse representation," *IEEE Access*, vol. 7, pp. 15404–15413, 2019, doi: 10.1109/ACCESS.2019.2894624.

[29] W. Si, Y. Wang, and C. Zhang, "2D-DOA and polarization estimation using a novel sparse representation of covariance matrix with COLD array," *IEEE Access*, vol. 6, pp. 66385–66395, 2018, doi: 10.1109/ACCESS.2018.2879051.

[30] Y. Yue, Z. Zhang, C. Zhou, F. Xing, and Z. Shi, "Closed-form two-dimensional DOA and polarization joint estimation using parallel non-collocated sparse COLD arrays," in *Proc. IEEE 12th Sensor Array Multichannel Signal Process. Workshop*, 2022, pp. 16–20.

[31] M. Huihui and T. Haihong, "Joint 2D-DOA and polarization estimation for sparse nonuniform rectangular array composed of spatially spread electromagnetic vector sensor," *J. Syst. Eng. Electron.*, vol. 31, no. 6, pp. 1116–1127, Dec. 2020, doi: 10.23919/JSEE.2020.000084.

[32] X. Wang, M. Huang, and L. Wan, "Joint 2D-DOD and 2D-DOA estimation for coprime EMVS–MIMO radar," *Circuits, Syst. Signal Process.*, vol. 40, no. 6, pp. 2950–2966, 2021, doi: 10.1007/s00034-020-01605-5.

[33] F. Wen, G. Gui, H. Gacanin, and H. Sari, "Compressive sampling framework for 2D-DOA and polarization estimation in mmWave polarized massive MIMO systems," *IEEE Trans. Wireless Commun.*, vol. 22, no. 5, pp. 3071–3083, May 2023, doi: 10.1109/TWC.2022.3215965.

[34] T. Shu, J. He, and V. Dakulagi, "3-D near-field source localization using a spatially spread acoustic vector sensor," *IEEE Trans. Aerosp. Electron. Syst.*, vol. 58, no. 1, pp. 180–188, Feb. 2022, doi: 10.1109/TAES.2021.3092703.

[35] P. P. Vaidyanathan and P. Pal, "Sparse sensing with co-prime samplers and arrays," *IEEE Trans. Signal Process.*, vol. 59, no. 2, pp. 573–586, Feb. 2011, doi: 10.1109/ACSSC.2010.5757766.

[36] P. Pal and P. P. Vaidyanathan, "Nested arrays: A novel approach to array processing with enhanced degrees of freedom," *IEEE Trans. Signal Process.*, vol. 58, no. 8, pp. 4167–4181, Aug. 2010, doi: 10.1109/TSP.2010.2049264.

[37] C.-L. Liu and P. P. Vaidyanathan, "Super nested arrays: Linear sparse arrays with reduced mutual coupling-Part I: Fundamentals," *IEEE Trans. Signal Process.*, vol. 64, no. 16, pp. 4203–4217, Aug. 2016, doi: 10.1109/TSP.2016.2558167.

[38] B. Liao and S.-C. Chan, "A cumulant-based method for direction finding in uniform linear arrays with mutual coupling," *IEEE Antennas Wireless Propag. Lett.*, vol. 13, no. 2, pp. 1717–1720, 2014, doi: 10.1109/LAWP.2014.2352939.

[39] G. Wang, Z. Fei, and S. Ren, "2D DOA estimation exploiting vertical synthetic planar arrays," *IEEE Access*, vol. 9, pp. 3497–3507, 2021, doi: 10.1109/ACCESS.2020.3047686.

[40] M. D. Zoltowski, M. Haardt, and C. P. Mathews, "Closed-form 2-D angle estimation with rectangular arrays in element space or beamspace via unitary ESPRIT," *IEEE Trans. Signal Process.*, vol. 44, no. 2, pp. 316–328, Feb. 1996.

[41] B. Friedlander and A. J. Weiss, "Direction finding in the presence of mutual coupling," *IEEE Trans. Antennas Propag.*, vol. 39, no. 3, pp. 273–284, Mar. 1991, doi: 10.1109/8.76322.

[42] I. J. Gupta and A. A. Ksienski, "Effect of mutual coupling on the performance of adaptive arrays," *Adapt. Antennas Wireless Commun.*, vol. 31, no. 5, pp. 785–791, Sep. 1983, doi: 10.1109/9780470544075.ch3.

[43] H. Singh, H. L. Sneha, and R. M. Jha, "Mutual coupling in phased arrays: A review," *Int. J. Antennas Propag.*, vol. 2013, pp. 1–23, 2013, doi: 10.1155/2013/348123.

[44] E. BouDaher, F. Ahmad, M. G. Amin, and A. Hoorfar, "Mutual coupling effect and compensation in non-uniform arrays for direction-of-arrival estimation," *Digit. Signal Process.*, vol. 61, pp. 3–14, 2017, doi: 10.1016/j.dsp.2016.06.005.

[45] E. BouDaher and A. Hoorfar, "Comparison of nature-inspired techniques in design optimization of non-uniformly spaced arrays in the presence of mutual coupling," *Digit. Signal Process.*, vol. 105, pp. 1–19, 2020, doi: 10.1016/j.dsp.2020.102780.

[46] J. Shi, G. Hu, X. Zhang, F. Sun, and H. Zhou, "Sparsity-based two-dimensional DOA estimation for coprime array: From sum-difference coarray viewpoint," *IEEE Trans. Signal Process.*, vol. 65, no. 21, pp. 5591–5604, Nov. 2017, doi: 10.1109/TSP.2017.2739105.

[47] S. K. Yadav and N. V. George, "Sparse 3D array made from nested linear array branches for underdetermined source localization," in *Proc. 30th Eur. Signal Process. Conf.*, 2022, pp. 1746–1750.

[48] M. Wang and A. Nehorai, "Coarrays, MUSIC, and the Cramér-Rao bound," *IEEE Trans. Signal Process.*, vol. 65, no. 4, pp. 933–946, Feb. 2017, doi: 10.1109/TSP.2016.2626255.

[49] P. Pal and P. P. Vaidyanathan, "Coprime sampling and the music algorithm," in *Proc. Digit. Signal Process. Signal Process. Educ. Meeting*, 2011, pp. 289–294, doi: 10.1109/DSP-SPE.2011.5739227.

[50] C. L. Liu and P. P. Vaidyanathan, "Cramér–Rao bounds for coprime and other sparse arrays, which find more sources than sensors," *Digit. Signal Process.*, vol. 61, pp. 43–61, 2017, doi: 10.1016/j.dsp.2016.04.011.

SALEH A. ALAWSH (Member, IEEE) received the B.Sc. degree in electronic and communications from Hadhramout University, Al Mukalla, Yemen, in 2007, and the M.Sc. degree in telecommunication and the Ph.D. degree from the King Fahd University of Petroleum and Minerals (KFUPM), Dhahran, Saudi Arabia, in 2013 and 2018, respectively. He is currently a Researcher with KFUPM. In 2013, he joined Electrical Engineering Department, KFUPM, as a Lecturer, His research interests include ultra-wideband systems, narrow band interference mitigation, direction-of-arrival estimation, localization, and compressive sensing. He was awarded the Best Laboratory Instructor with the Department of Electrical Engineering, KFUPM.

MOHAMED H. MOHAMED received the B.Sc. degree in electrical engineering from the King Fahd University of Petroleum and Minerals, Dhahran, Saudi Arabia, in 2022. His main research interests include signal processing, machine learning, and direction-of-arrival estimation.

IBRAHIM ABOUMAHMOUD received the B.Sc. and M.Sc. degrees from the King Fahd University of Petroleum and Minerals, Dhahran, Saudi Arabia, in 2019 and 2021, respectively. His main research interests include signal processing and direction-of-arrival estimation.

MOHAMMAD ALHASSOUN (Member, IEEE) received the B.Sc. degree in electrical engineering from the King Fahd University of Petroleum and Minerals (KFUPM), Dhahran, Saudi Arabia, in 2013, and the M.S. and Ph.D. degrees from the Georgia Institute of Technology, Atlanta, GA, USA, in 2015 and 2019, respectively. He is currently an Assistant Professor with KFUPM. He was with the Nokia Bell Laboratories as an EMCD Intern and a Graduate Assistant with KFUPM. His research interests include radio-channel modeling, retrodirective backscatter communications, spectrally-efficient backscatter systems, and physical-layer applications of machine learning. He was the recipient of the 2018 and 2019 IEEE International Conference on RFID Best Paper Award. He was awarded the Best Laboratory Instructor at the Department of Electrical Engineering, KFUPM. He was also awarded the Tech to Teaching Certificate at the College Teaching, Georgia Institute of Technology, in addition to the Associate Level Certificate from the Center of Integration of Research, Teaching and Learning.

ALI H. MUQAIBEL (Senior Member, IEEE) received the Ph.D. degree from Virginia Polytechnic Institute, State University, Blacksburg, VA, USA, in 2003. He is a Professor with the Electrical Engineering Department, King Fahd University of Petroleum and Minerals, Dhahran, Saudi Arabia. He is the Director of the Interdisciplinary Research Center for Communication Systems and Sensing. During his study with Virginia Tech, he was with the Time Domain and RF Measurements Laboratory and the Mobile and Portable Radio Research Group. He was a Visiting Associate Professor with the Center of Advanced Communications, Villanova University, Villanova, PA, USA, in 2013, a Visiting Professor with the Georgia Institute of Technology, Atlanta, GA, USA, in 2015, and a Visiting Scholar with the King Abdullah University for Science and Technology, Thuwal, Saudi Arabia, in 2018 and 2019. He has authored two book chapters and more than 140 articles. His research interest include communications and sensing applications, including the direction of arrival estimation, through-wall-imaging, localization, channel characterization, and ultra-wideband signal processing. He was the recipient of many awards in the excellence in teaching, advising, and instructional technology.